Contrib Mineral Petrol (2000) 138: 51–58

Joseph M. Pyle · Frank S. Spear

An empirical garnet (YAG) – xenotime thermometer

Received: 21 January 1999 / Accepted: 13 September 1999

Abstract A pronounced negative correlation between the yttrium concentration in garnet ($[Y]_{Grt}$) and temperature has been observed in xenotime (YPO_4)-bearing metapelites from central New England, USA. The $[Y]_{Grt}$ decreases roughly two orders of magnitude (~5500 to less than 100 ppm Y) over a 150 °C interval. A regression of $\ln([Y]_{Grt})$ against estimated reciprocal temperature yields the following relationship:

$$\ln(\text{ppm Y in garnet}) = 16031(\pm 862)/T - 13.25(\pm 1.12)$$

with $R^2 = 0.97$. The decrease in garnet Y content is most rapid over garnet- to staurolite-zone conditions (450–550 °C) and the thermometer has a precision of a few degrees in this range.

Introduction

The sensitivity of trace elements to changes in external (*P*, *T*, *X*, mineral assemblage) conditions and resistance of trace elements to diffusive reequilibration has been well documented by previous workers (e.g., Lanzirotti 1995; Schwandt et al. 1996; Spear and Kohn 1996). Given these inherent properties, calibration of trace element thermobarometers has the potential to uncover previously unobtainable portions of the *P-T* histories of metamorphic rocks.

In this paper we present an empirical trace element geothermometer that utilizes the concentration of yttrium in garnet ($[Y]_{Grt}$) in xenotime (YPO_4)-bearing pelites. The assumption made throughout this paper is that the presence of xenotime assures a buffered value of a_{YPO4}, and that equilibrium garnet growth during a period of xenotime stability implies garnet growth under buffered a_{YPO4}. Arguments for garnet growth in equilibrium with xenotime are presented, a garnet-xenotime thermometer is developed, and applications and limitations of the thermometer are discussed.

J.M. Pyle (✉) · F.S. Spear
Department of Earth and Environmental Sciences,
Rensselaer Polytechnic Institute, Troy, NY12180, USA

Editorial responsibility: K.V. Hodges

Sample selection and regional setting

A well-characterized suite of garnet- to migmatite-zone pelites were selected for study. This suite is part of the Ordovician and Silurian metasediments of the Bronson Hill anticlinorium and adjacent Merrimack Synclinorium, west-central New Hampshire (Spear 1992), a nappe-and-thrust complex that underwent later (dome-stage) folding (Thompson et al. 1968; Robinson et al. 1991; Spear 1992). Samples belonging to the New Hampshire suite are labeled BF, 89, or 93. Additional calibrant samples include calcic (epidote ± sphene-bearing) pelites (labeled TM) from the Strafford Dome, VT, area (Menard and Spear 1993) and a single staurolite–kyanite-zone pelite (SP-9B1) from the Cordillera Darwin, Chile (Kohn et al. 1993).

Temperature estimates of calibrant samples

The samples examined in this study have been extensively characterized in previous studies (Spear et al. 1990; Kohn et al. 1993; Menard and Spear 1993; Spear et al. 1995; Kohn et al. 1997; Table 1). Metamorphic temperatures, pressures and *P-T* paths have been inferred from garnet-biotite thermometry, garnet-plagioclase barometry and Gibbs method modeling. Pressures and temperatures are estimated to be accurate to ± 30 °C and ± 1 kbar (Table 1).

Analytical methods

Thirteen xenotime-bearing samples were selected for detailed accessory phase identification, element distribution mapping, and quantitative analysis on the JEOL

Table 1 Garnet compositions and [a]thermobarometry estimates for calibrant samples

Sample	BF-17	TM-549	93-19A	BF-38B	TM-445	SP-9B1	89-9	89-9	89-22	89-22	BF-78
Reference[b]	Core 1	Core 2	Core 1	Core 3	Rim 2	Rim 4	Core 5	Rim 5	Core 5	Rim 5	Rim 5
P (bars)	4000	5000	3800	5000	7000	6000	3000	4500	3000	5000	2800
T (°C)	460	480	495	510	550	550	530	600	580	535	610
SiO_2	36.70	36.95	37.04	36.88	37.46	38.09	37.51	37.50	36.70	36.97	37.13
Al_2O_3	21.12	21.26	20.58	20.85	21.40	21.81	21.37	21.37	21.56	20.70	21.38
FeO	28.56	23.98	34.54	29.41	34.00	32.98	28.42	29.42	36.10	38.34	31.72
MgO	1.41	1.56	1.42	1.58	3.38	3.56	2.96	2.96	2.34	2.30	2.44
MnO	7.91	14.03	5.22	8.63	2.46	2.79	8.71	7.95	3.34	1.44	6.90
CaO	4.67	2.92	1.50	2.64	2.33	3.08	1.34	1.47	1.27	1.45	1.01
Ppm Y	5346 (250)	4030 (648)	2149 (57)	1217 (45)	629 (76)	563 (56)	532 (86)	209 (71)	241 (44)	619 (51)	123 (33)
Ppm P	<100	112 (20)	<100	110 (25)	<100	<100	<100	<100	<100	<100	230 (19)
Total	101.06	101.24	100.57	100.17	101.12	102.39	100.39	100.70	101.35	101.29	100.65
[c]X_{prp}	0.0552	0.0618	0.0570	0.0634	0.1323	0.1375	0.1192	0.1182	0.0921	0.0895	0.0981
X_{alm}	0.6277	0.5324	0.7770	0.6617	0.7464	0.7147	0.6418	0.6589	0.7969	0.8370	0.7150
X_{sps}	0.1761	0.3155	0.1189	0.1966	0.0547	0.0612	0.1992	0.1803	0.0747	0.0318	0.1575
X_{grs}	0.1315	0.0831	0.0432	0.0761	0.0655	0.0855	0.0388	0.0422	0.0359	0.0406	0.0292
X_{YAG}	0.0095	0.0072	0.0039	0.0022	0.0011	0.0010	0.0010	0.0004	0.0004	0.0011	0.0002

[a] Garnet-biotite Fe-Mg geothermometry (Ferry and Spear 1978; Hodges and Spear 1982; Berman 1990); Garnet-muscovite-biotite-plagioclase and garnet-aluminosilicate-plagioclase-quartz geobarometry (Hodges and Crowley 1985)
[b] (*1* unpublished data, *2* Menard and Spear 1993, *3* Spear et al. 1990, *4* Kohn et al. 1993, *5* Spear et al. 1995)
[c] $X_i = i/(\mathrm{Mg} + \mathrm{Fe} + \mathrm{Mn} + \mathrm{Ca} + \mathrm{Y})$, where i = Mg, Fe, Mn, Ca, Y

733 Superprobe at Rensselaer Polytechnic Institute. Accessory phases were identified using back-scattered electron imaging and the automated EDS software package QuantumX, and sample images were captured with imaging software package dPict (Geller Microanalytical Co.).

Element distribution maps were created with the automated mapping package Xraymap (coded by F. Spear and D. Wark). Operating conditions for map collection include an accelerating voltage of 15 kV, cup current of 1.5–2.0 μA, step size of 5–10 μm/pixel, and dwell time of 0.05–0.1 s/pixel; images were processed with the public domain program NIH Image v. 1.61b12 (developed at the National Institutes of Health and available for downloading on the Internet at http://rsb.info.nih.gov/nih-image/).

Quantitative analyses were performed using the Geller Microanalytical quantitative analysis software package dQant, utilizing a ZAF matrix correction routine using machine settings listed in Table 2. Baseline and window width were set using pulse-height analysis to minimize second- and higher-order peak interference from major elements, and background collection positions were set to minimize major element interference. The electron microprobe trace element detection limit (ca. 100 ppm) was calculated using detectability limit equations found in Goldstein et al. (1984). Garnets were analyzed for Y and P (Table 1) using synthetic YPO_4 and $ScPO_4$ as standards for Y and P, respectively (Jarosewich and Boatner 1991). Average cup current was ~500 nA, with 20 second counting on peak, and 20 second counting on background. Trace element concentrations (Table 1) represent the average of 5 spot analyses collected in a region of approximately 400 μm^2 (20×20 μm), with values in parentheses showing the standard deviation of the average concentration. Xenotime was analyzed for Ca, Si, P, Th, U, Pb, La, Ce, Pr, Nd, Sm, Gd, Dy Er, Ho, Yb, and Y (Table 3). Operating conditions included an accelerating voltage of 15 kV, cup current of 50 nA, dwell times of 20 seconds each on peak and background. Between 3 and 11 spots were analyzed on individual grains, and analyses presented in Table 3 are representative of each sample.

Results

Xenotime occurs in three distinct textural habits in the sample suite (Fig. 1; see also Pyle and Spear 1998, and J.M. Pyle and F.S. Spear in review): (1) as inclusions within garnet cores (Fig. 1a); (2) as distinct matrix grains (Fig. 1b); (3) as inclusions within phases replacing garnet, i.e., chlorite, biotite, or muscovite that truncates, cross-cuts, or completely replaces former garnet (“reaction-zone xenotime”; Fig. 1c, d). Xenotime inclusions in garnet occur at all metamorphic grades below anatexis. Matrix xenotime, where present, is more abundant in garnet-zone samples (maximum 0.5–1.0 modal%) than in higher-grade (staurolite-zone or sillimanite-zone) samples (maximum 0.1 modal%).

Xenotime is assumed to be in equilibrium with garnet based on the following criteria. Where matrix xenotime is present in garnet-grade samples, it is assumed that garnet was in equilibrium with xenotime throughout the entire period of garnet growth. For garnet-zone samples with xenotime present only as garnet core inclusions, it is assumed that only the core of the garnet grew in equi-

Table 2 Analysis setup and operating conditions for garnet and xenotime

Element	Line	Standard	Crystal	Bkg high (+Δmm)	Bkg low (−Δmm)	Bias (V)	Baseline (V)	Window (V)
Garnet								
Y	Lα	YPO_4	TAP	−1[a]	1	1700	1.0	2.5
P	Kα	$ScPO_4$	TAP	2	2	1700	1.0	2.5
Xenotime								
Ca	Kα1	Apatite	PET	1.0	2.0	1700	1.5	5.0
P	Kα1	Apatite	TAP	5.0	−5.0[a]	1700	0.8	3.2
Si	Kα1	$ThSiO_4$	TAP	3.5	2.9	1700	1.0	8.0
Th	Mα1	$ThSiO_4$	PET	2.5	3.5	1700	0.5	5.0
U	Mα1	UO_2	PET	3.0	3.5	1700	1.0	6.0
Pb	Mα1	PbS	PET	4.0	4.0	1700	1.0	5.0
La	Lα1	$LaPO_4$	LiF	2.0	2.0	1700	1.0	5.0
Ce	Lα1	$CePO_4$	LiF	2.0	2.0	1700	1.0	5.0
Pr	Lβ1	$PrPO_4$	LiF	1.5	1.5	1700	1.0	5.0
Nd	Lα1	$NdPO_4$	LiF	2.0	2.5	1700	1.0	5.0
Sm	Lβ1	$SmPO_4$	LiF	1.5	4.5	1700	1.0	5.0
Gd	Lβ1	$GdPO_4$	LiF	1.2	1.0	1700	1.0	5.0
Dy	Lβ1	$DyPO_4$	LiF	1.1	−1.0	1700	1.0	5.0
Ho	Lβ1	$HoPO_4$	LiF	3.3	7.0	1700	1.0	5.0
Er	Lα1	$ErPO_4$	LiF	3.3	1.0	1700	1.0	5.0
Yb	Lα1	$YbPO_4$	LiF	1.6	8.7	1700	1.0	5.0
Y	Lα1	YPO_4	LiF	3.0	−3.0	1700	0.8	3.2

[a] Negative value for background (*Bkg*) indicates that both background measurements were taken on the same side of the peak measurement in order to prevent major element peak interferences

librium with xenotime. Xenotime present in reaction zones (as defined above) is most likely produced during garnet-consuming reactions, and interpreted not to have been in equilibrium with garnet.

Concentrations of yttrium in garnet crystals that are interpreted to have been in equilibrium with xenotime are shown as a function of P and T in Fig. 2. There is a strong correlation between yttrium concentration and temperature with $[Y]_{Grt}$ decreasing from nearly 5350 ppm at an estimated temperature of 460 °C to approximately 120 ppm at an estimated temperature of 610 °C, a decrease of nearly 2 orders of magnitude over a 150 °C temperature interval. The isopleths, which have been drawn by inspection, are steep (ca. 150 bars/degree) and imply little pressure dependence of $[Y]_{Grt}$, although the range of pressures of the samples is not large.

The natural log of the yttrium concentration in garnet has been regressed against reciprocal temperature with the following result (Fig. 3):

$$\ln(\text{ppm Y in garnet}) = \frac{16031(\pm 862)}{T(\text{K})} - 13.25(\pm 1.12) \quad (1)$$

with a calculated $R^2 = 0.97$. Equal weights for all data points were assumed and standard errors on the slope (σ_m) and intercept (σ_b) were estimated using only $\sigma_{[Y]Grt}$. A linear regression was also performed against $1/T$ and P, but the fit was not substantially improved

Table 3 Xenotime analyses from calibrant samples

Sample	BF-17	TM-549	93-19A	BF-38B	TM-445	SP-9B1	89-9	89-22	BF-78
SiO_2	1.71	0.15	0.22	0.75	0.26	0.70	0.62	0.16	0.20
CaO	0.23	0.06	0.02	0.10	0.13	0.10	0.07	0.09	0.04
P_2O_5	36.34	35.78	36.07	35.72	36.37	35.65	35.87	36.23	36.67
UO_2	<0.01	0.09	<0.01	0.21	0.68	0.03	0.25	0.39	<0.01
ThO_2	0.13	0.12	0.22	0.05	<0.01	<0.01	0.07	<0.01	<0.01
PbO	0.56	0.46	0.47	0.40	0.34	0.24	0.50	0.41	0.28
La_2O_3	0.04	0.02	0.07	<0.01	0.01	<0.01	<0.01	<0.01	<0.01
Ce_2O_3	0.08	0.02	<0.01	<0.01	0.04	0.11	<0.01	0.01	<0.01
Pr_2O_3	<0.01	0.12	<0.01	<0.01	<0.01	0.11	0.06	<0.01	0.04
Nd_2O_3	0.31	0.39	0.15	0.32	0.27	0.24	0.15	0.37	0.27
Sm_2O_3	<0.01	0.10	0.15	<0.01	0.23	<0.01	<0.01	0.16	<0.01
Dy_2O_3	5.65	6.31	6.40	5.80	7.20	2.89	3.28	5.71	5.60
Yb_2O_3	3.01	3.29	4.25	3.92	0.93	7.64	6.81	3.65	4.90
Er_2O_3	3.23	4.20	4.52	4.18	3.13	4.95	5.55	4.39	4.91
Gd_2O_3	2.89	3.70	4.79	3.68	4.40	2.53	2.49	3.65	3.47
Ho_2O_3	0.94	1.41	1.18	1.38	1.64	1.18	1.13	1.31	1.47
Y_2O_3	44.03	43.80	41.80	42.68	46.03	43.68	43.82	44.12	43.86
Total	99.14	100.02	100.31	99.19	101.66	100.05	100.66	100.64	101.71
X_{YPO_4}[a]	0.8073	0.7819	0.7588	0.7795	0.7993	0.7729	0.7841	0.7846	0.7772

[a] $X_{YPO_4} = Y/(Y + Ca + Pb + Th + U + La + Ce + Pr + Nd + Sm + Dy + Er + Gd + Ho + Yb)$

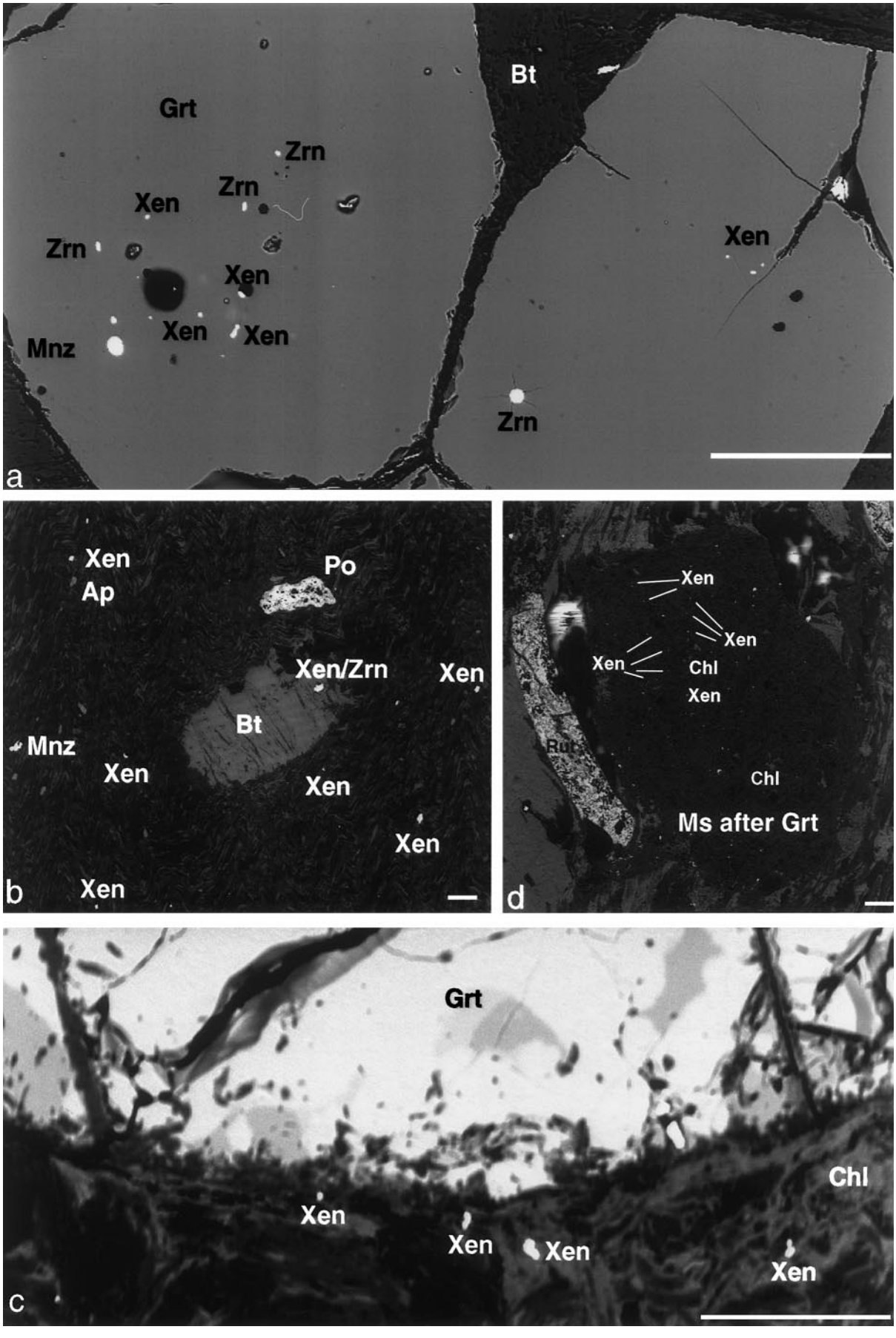
Grt
Bt
Zrn
Zrn
Xen
Zrn
Xen
Xen
Xen
Mnz
Xen
Zrn
a
Xen
Ap
Po
Xen/Zrn
Xen
Bt
Mnz
Xen
Xen
Xen
b
Xen
Xen
Xen
Xen
Chl
Xen
Rut
Chl
Ms after Grt
d
Grt
Chl
Xen
Xen
Xen
Xen
c

◀

Fig. 1 BSE images showing the textural habits of xenotime in pelites. **a** Xenotime inclusions in garnet core, sample BF-78 (sillimanite zone). **b** Matrix xenotime, sample 93-19A (garnet zone). **c** Xenotime grains in chlorite-filled reaction zones around garnet, sample 93-19A (garnet zone). **d** Xenotime grains in muscovite pseudomorph after garnet, sample 92-53 (garnet zone). (*Grt* garnet, *Bt* biotite, *Xen* xenotime, *Mon* monazite, *Zrn* zircon, *Ap* apatite, *Po* pyrrhotite, *Xen*/*Zrn* zircon with xenotime overgrowth, *Rut* rutile). All scale *bars* 100 μm

and it was decided that the range in pressures in the calibrant data set did not warrant incorporating a pressure correction.

Thermodynamic basis for the xenotime-garnet thermometer

The goodness of fit of Eq. (1) (Fig. 3) suggests that the yttrium concentration in garnet in equilibrium with xenotime is valid as a thermometer. The relationship is strictly empirical, but suggests that there is a thermodynamic basis that controls $[Y]_{Grt}$.

Reactions have been identified that can be used as a thermodynamic basis for the above empirical relationship, although, as will be discussed, each suffers from practical difficulties that warrant them unsuitable as thermometers. Any reaction that involves both xenotime (YPO_4) and the YAG component of garnet ($Y_3Al_2Al_3O_{12}$; Jaffe 1951; Yoder and Keith 1951) must balance phosphorus in addition to yttrium. Two components available in pelites for balancing P in xenotime are apatite and a P-garnet component, which give rise to three independent reactions with associated equilibrium constants:

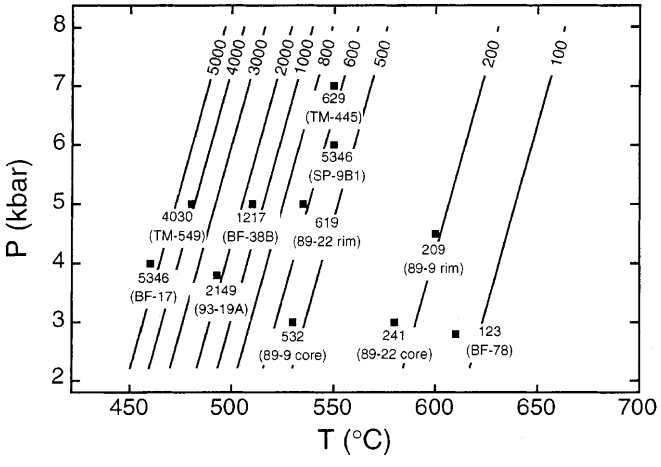

Fig. 2 *P-T* plot of eleven garnet yttrium analyses from nine xenotime-bearing pelites. Pressure and temperature estimated using garnet-biotite thermometry (Hodges and Spear 1982; Ferry and Spear 1978; Berman 1990) and garnet-muscovite-biotite-plagioclase and garnet-aluminosilicate-plagioclase barometry (Hodges and Crowley 1985) (Table 1). *Labels* indicate concentration of Y in garnet (ppm). *Lines* are contours of $[Y]_{Grt}$ drawn by inspection

$$\underset{\text{YAG (in Grt)}}{Y_3Al_2Al_3O_{12}} + \underset{\text{OH-Apatite}}{Ca_5(PO4)_3(OH)} + 25/4\ \underset{\text{Qtz}}{SiO_2} = \underset{\text{Xen}}{3YPO_4} + 5/4\underset{\text{grs (in Grt)}}{Ca_3Al_2Si_3O_{12}} + 5/4\underset{\text{an (in Plg)}}{CaAl_2Si_2O_8} + 1/2\underset{\text{fluid}}{H_2O} \quad (2)$$

$$K_2 = \frac{a^{5/4}_{grs,Grt}\, a^{5/4}_{an,Plg}\, a^{3}_{YPO_4,Xen}\, f^{1/2}_{H_2O}}{a_{YAG,Grt}\, a_{OH-Ap}} \quad (2a)$$

$$\underset{\text{an (in Plg)}}{6\,CaAl_2Si_2O_8} + \underset{\text{Xen}}{3YPO_4} = \underset{\text{P-grt (in Grt)}}{2Ca_3Al_2Al_{1.5}P_{1.5}O_{12}} + \underset{\text{YAG (in Grt)}}{Y_3Al_2Al_3O_{12}} + 12\ \underset{\text{Qtz}}{SiO_2} \quad (3)$$

$$K_3 = \frac{a^{2}_{P,Grt}\, a_{YAG,Grt}}{a^{6}_{an,Plg}\, a^{3}_{YPO_4,Xen}} \quad (3a)$$

$$\underset{\text{grs (in Grt)}}{2Ca_3Al_2Si_3O_{12}} + \underset{\text{Als}}{4Al_2SiO_5} + \underset{\text{Xen}}{3YPO_4} = \underset{\text{P-grt (in Grt)}}{2Ca_3Al_2Al_{1.5}P_{1.5}O_{12}} + \underset{\text{YAG (in Grt)}}{Y_3Al_2Al_3O_{12}} + 10\ \underset{\text{Qtz}}{SiO_2} \quad (4)$$

$$K_4 = \frac{a^{2}_{P,Grt}\, a_{YAG,Grt}}{a^{2}_{grs,Grt}\, a^{4}_{Al_2SiO_5}\, a^{3}_{YPO_4,Xen}} \quad (4a)$$

Each expression involves the activity of YPO_4 in xenotime. Typical pelitic xenotime has X_{YPO4} between 0.7 and 0.8 (e.g., Franz et al. 1996; Heinrich et al. 1997). All xenotime analyses from our data set fall in this range (Table 3). Therefore, the activity of YPO_4 in xenotime is approximately constant for the sample suite, and is expected to be approximately constant in all pelitic xenotime.

Equation (2) balances P with apatite and requires the activity of hydroxy-apatite in the equilibrium constant. Inclusion of hydroxy-apatite in (2) is problematic in that pelitic apatite incorporates a significant amount of fluoroapatite component (Finger et al. 1998), and at low grades may be virtually pure F-apatite (W. Heinrich, personal communication, 1999). Semi-quantitative analysis of F in apatite from our calibrant suite yielded values of $X_{FAp} = 0.85$ to 0.99. Furthermore, accurate measurement of the F concentration in apatite is difficult using the electron microprobe (e.g., Stormer et al. 1993).

Equations (3) and (4) balance P using a phosphorous garnet component. Assuming P resides on the Z (tetrahedrally coordinated) site in garnet (Meagher 1982), an appropriate component is $Ca_3Al_2Al_{1.5}P_{1.5}O_{12}$. Both (3) and (4) are anhydrous, obviating the necessity for estimates of fluid composition and/or fugacity, and both are applicable over a wide range of sample grades. If the aluminosilicate-bearing reaction is used, and $a_{Al2SiO5}$ is assumed to be equal to 1, then the thermometer application requires compositional measurements of garnet and xenotime only. For Al_2SiO_5-absent assemblages, the $a_{Al2SiO5}$ may be calculated following Ghent and Grover (1995).

The problem encountered in using reactions (3) or (4) as a basis for the garnet-xenotime thermometer is the low solubility of phosphorus in garnet. Maximum garnet

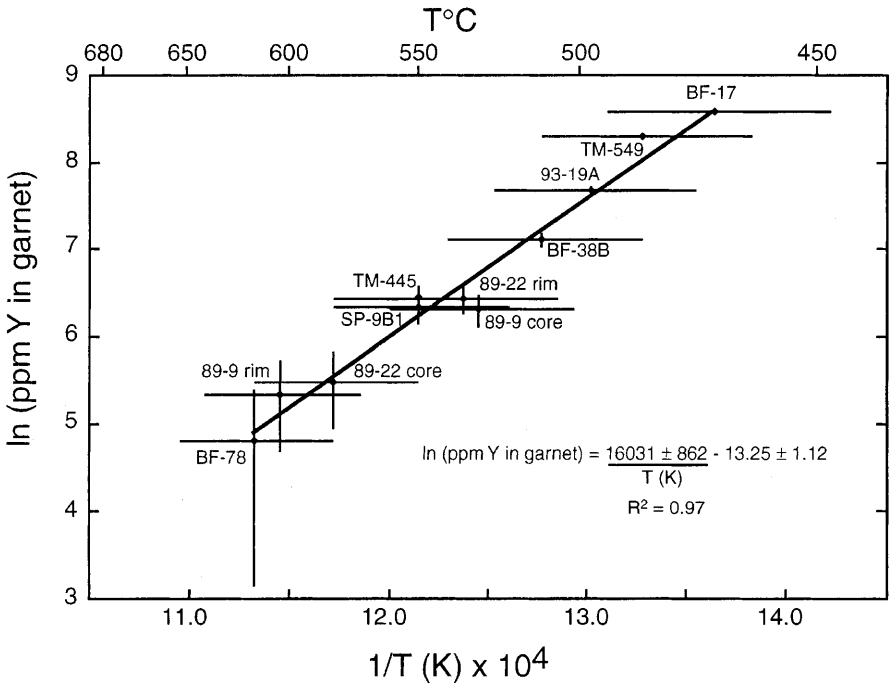

Fig. 3 Plot of ln(ppm Y in garnet) versus reciprocal absolute temperature in xenotime-bearing pelites. Result of linear regression is shown on plot. In samples 89-9 and 89-22, temperature estimates were made for both garnet core and rim. Error *bars* represent assumed accuracy measurements on temperature estimates from thermobarometry (±30 °C) and electron microprobe measurements of garnet composition (±100 ppm Y)

phosphorus content in these samples is approximately 230 ppm (BF-78) and most garnet samples analyzed contain less than 100 ppm P (Table 1). Assuming a precision of ±100 ppm on garnet analyses introduces $X_{P,Grt}$ uncertainties on the order of 75% or greater, which drastically limits the effectiveness of reactions (3) or (4) as a thermometer.

The primary difficulty with each of these equilibria for use as a thermometer is that they involve greatly increased uncertainties in the calculated value of the equilibrium constant, which render the thermometer far less precise. The strictly empirical relationship (Eq. 1) carries relatively small uncertainties, especially at low temperature where $[Y]_{Grt}$ is several thousand ppm. Nevertheless, these relations demonstrate that there are valid thermodynamic controls on $[Y]_{Grt}$, in support of the use of Eq. 1 as a thermometer.

Discussion

It is to be emphasized that the correlation of $[Y]_{Grt}$ with temperature is empirical and ideally would involve a considerably larger sample base for calibration. Accuracy of temperatures calculated from this thermometer are no better than the accuracy of the temperature estimates of the calibrant samples: i.e. on the order of ±30 °C.

Precision of temperatures calculated from the thermometer, however, is considerably better, because they involve only propagation of uncertainties in the concentration of yttrium in garnet. The greatest rate of decrease of $[Y]_{Grt}$ occurs between lower garnet-zone and staurolite-zone conditions (Fig. 4), so the thermometer is considerably more precise at low temperatures. Assuming a measurement error of ±100 ppm Y (a typical electron microprobe uncertainty), precision of temperature estimates can be evaluated graphically from Figs. 3 or 4 as follows: for a lower garnet-zone garnet (~4000 ppm Y), σ_T = ±1 °C; upper garnet-zone garnet (~1000 ppm Y), σ_T = ±4 °C; sillimanite-zone garnet (~150 ppm Y), σ_T = ±40 °C. Thus, the thermometer is best suited for application to garnet- and staurolite-zone xenotime-bearing pelites. More sensitive analyses of $[Y]_{Grt}$ (e.g., ion probe or LA-ICP-MS) would greatly improve the precision of temperature estimates in higher-grade samples.

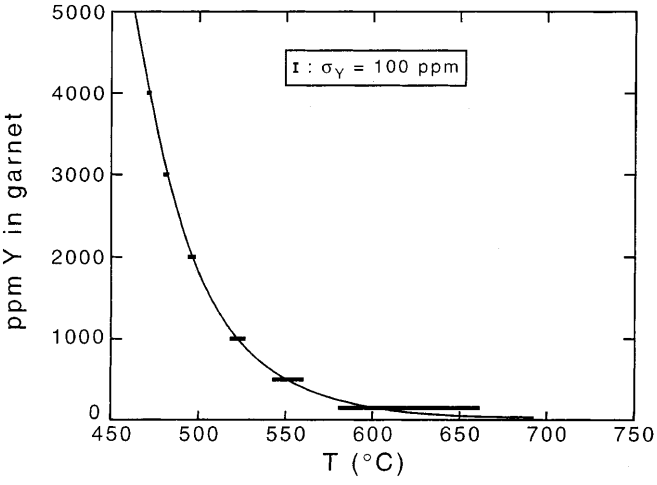

Fig. 4 Graphical representation of the garnet-xenotime thermometer as a plot of garnet composition (ppm Y in garnet) versus calculated temperature, using the regression from Fig. 3. *Bars* show precision of temperature estimate at different Y concentrations assuming $\sigma_{[Y]Grt}$ = ±100 ppm

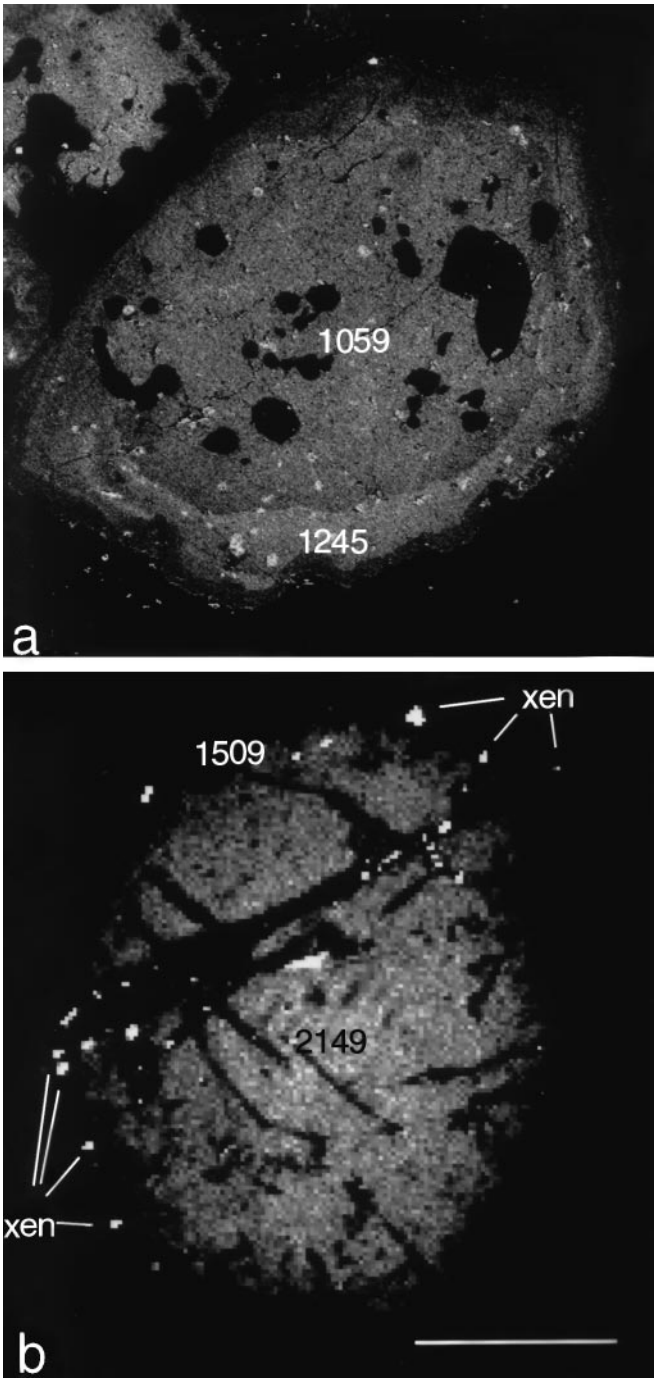

Fig. 5 a Yttrium distribution map for garnet, sample BF-14P (migmatite zone). Near-rim region of high yttrium content (1245 ppm) grew during vapor-absent melting of biotite (Kohn et al. 1997) at $T \sim 750$ °C; crystallization of melt resulted in consumption of garnet and xenotime precipitation. Relict garnet core is xenotime-bearing, and application of the garnet-xenotime thermometer to the core (1059 ppm Y) yields a temperature of 520 ± 4 °C. Garnet is approximately 8 mm across. **b** Yttrium distribution map for garnet, sample 93-19A (garnet zone). Sample contains matrix xenotime and garnet is smoothly zoned in yttrium from core (2149 ppm Y) to rim (1509 ppm Y). Application of the garnet-xenotime thermometer to this garnet yields a core-rim ΔT of 13 ± 4 °C. Scale *bar* = 100 μm

Potential applications

The empirical garnet-xenotime thermometer may also be used to identify low-grade relict garnet in samples that have undergone multiple generations of garnet growth. As an example of this application, five generations of garnet growth were identified in anatectic samples K92-12D and BF-14P from near Bellows Falls, Vermont (Kohn et al. 1997), through a combination of textural and compositional observations. A large (≈1 cm) porphyroblastic garnet in sample BF-14P with high Y, Sc, and Cr rims grown during anatexis contains a xenotime-bearing core with $[Y]_{Grt}$ = 1059 ppm (Fig. 5a). The estimated temperature for the core of this garnet is 520 ± 4 °C, over 200 °C below the estimated peak temperature of ~750 °C. All major element compositional record of this low-grade garnet crystallization event has been eradicated by diffusional reequilibration at or near the peak *P-T* conditions, but the resistance of Y in garnet to diffusive re-equilibration allows for identification of a specific portion of the prograde *P-T* path.

The garnet-xenotime thermometer is quite sensitive in the temperature range of the garnet-zone. A second application of this thermometer is calculation of the temperature difference between garnet core and rim in garnet zone samples. Sample 93-19A from western New Hampshire (Fig. 5b) contains matrix xenotime and garnet that is smoothly zoned in Y from core to rim, and has no obvious textural or compositional evidence for a growth hiatus. Using core and rim compositions of 2149 and 1509 ppm Y, respectively, a core-rim ΔT estimate of 13 ± 4 °C (493–506 °C) is retrieved (error estimate from ±100 ppm Y analytical precision). The largest garnet in this sample, with a core composition of 2386 ppm Y and rim composition of 1304 ppm Y, yields a ΔT of 23 ± 4 °C. A potentially useful application of this high-temperature sensitivity is to pair the calculated ΔT with measurement of the age of garnet core and rim to infer garnet growth rates and heating rates.

Acknowledgements This paper has benefited from constructive reviews by W. Heinrich, M.L. Williams, and the editorial handling of K.V. Hodges. D. Wark is thanked for maintenance of and analytical assistance on the JEOL 733 Superprobe at RPI. Funding for this research was provided by NSF grants EAR-9706463 and EAR-9903036 (to F.S.S).

References

Berman RG (1990) Mixing properties of Ca-Mg-Fe-Mn garnets. Am Mineral 75: 328–344

Ferry JM, Spear FS (1978) Experimental calibration of the partitioning of Fe and Mg between biotite and garnet. Contrib Mineral Petrol 66: 113–117

Finger F, Broska I, Roberts MP, Schermaier A (1998) Replacement of primary monazite by apatite-allanite-epidote coronas in an amphibolite facies granite gneiss from the eastern Alps. Am Mineral 83: 248–258

Franz G, Andrehs G, Rhede D (1996) Crystal chemistry of monazite and xenotime from Saxothuringian-Moldanubian metapelites, NE Bavaria, Germany. Eur J Mineral 8: 1097–1118

Ghent ED, Grover TW (1995) Calculation of the activity of Al_2SiO_5: applications to the geobarometry and hygrometry of garnet- and staurolite-zone pelitic rocks. Am J Sci 295: 923–942

Goldstein J, Newbury D, Echlin P, Joy D, Fiori D, Lifshin E (1984) Scanning electron microscopy and X-ray microanalysis. Plenum, New York

Heinrich W, Andrehs G, Franz G (1997) Monazite-xenotime miscibility gap thermometry. I. An empirical calibration. J Metamorphic Geol 15: 3–16

Hodges KV, Crowley PD (1985) Error estimation and empirical geothermobarometry for pelitic systems. Am Mineral 70: 702–709

Hodges KV, Spear FS (1982) Geothermometry, geobarometry, and the Al_2SiO_5 triple point at Mt. Moosilauke, New Hampshire. Am Mineral 67: 1118–1134

Jaffe HW (1951) The role of yttrium and other minor elements in the garnet group. Am Mineral 36: 133–155

Jarosewich E, Boatner LA (1991) Rare-earth element reference samples for electron microprobe analysis. Geostand Newsl 15: 397–399

Kohn MJ, Spear FS, Dalziel IWD (1993) Metamorphic *P-T* paths from Cordillera Darwin, a core complex in Tierra del Fuego, Chile. J Petrol 34: 519–542

Kohn MJ, Spear FS, Valley JW (1997) Dehydration-melting and fluid recycling during metamorphism: Rangely formation, New Hampshire, USA. J Petrol 38: 1255–1277

Lanzirotti A (1995) Yttrium zoning in metamorphic garnets. Geochim Cosmochim Acta 59: 4105–4110

Meagher EM (1982) Silicate garnets. (Reviews in mineralogy 5, 2nd edn) Mineral Soc Am, Washington, DC, pp 25–66

Menard T, Spear FS (1993) Metamorphism of calcic pelitic schists, Strafford Dome, Vermont: compositional zoning and reaction history. J Petrol 34: 977–1005

Pyle JM, Spear FS (1998) Trace element distributions in garnet: a road map for following pelite reaction histories. In: Geol Soc Am 1998 Annu Meet Abstr Program, A231

Pyle JM, Spear FS (1999) Yttrium zoning in garnet: coupling of major and accessory phases during metamorphic reactions. Geol Mater Res, in review

Robinson P, Thompson PJ, Elbert DC (1991) The nappe theory in the Connecticut Valley region: thirty-five years since Jim Thompson's first proposal. Am Mineral 76: 689–712

Schwandt CS, Papike JJ, Shearer CK (1996) Trace element zoning in pelitic garnet of the Black Hills, South Dakota. Am Mineral 81: 1195–1207

Spear FS (1992) Inverted metamorphism, *P-T* paths, and the cooling history of west-central New Hampshire: implications for the tectonic evolution of central New England. In: Robinson P, Brady J (eds) Guidebook for fieldtrips in the Connecticut Valley region of Massachusetts and the adjacent States, vol 2. Dep Geol Geogr Univ Massachusetts, Amherst, pp 446–466

Spear FS, Kohn MJ (1996) Trace element zoning in garnet as a monitor of crustal melting. Geology 24: 1099–1102

Spear FS, Hickmott DD, Selverstone J (1990) Metamorphic consequences of thrust emplacement, Fall Mountain, New Hampshire. Geol Soc Am Bull 102: 1344–1360

Spear FS, Kohn MJ, Paetzold S (1995) Petrology of the regional sillimanite zone, west-central New Hampshire, U.S.A., with implications for the development of inverted isograds. Am Mineral 80: 361–376

Stormer JCJr, Pierson MJ, Tacker RC (1993) Variation of F and Cl X-ray intensity due to anisotropic diffusion of apatite during electron microprobe analysis. Am Mineral 78: 641–648

Thompson JBJr, Robinson P, Clifford TN, Trask NJ (1968) Nappes and gneiss domes in west-central New England. In: Zen E-an, White WS, Hadley JB, Thompson JBJr (eds) Studies of Appalachian geology, Northern and Maritime. John Wiley and Sons, New York, pp 319–327

Yoder HS, Keith ML (1951) Complete substitution of aluminum for silicon: the system $3MnO{\cdot}Al_2O3{\cdot}3SiO_2 - 3Y_2O_3{\cdot}5Al_2O_3$. Am Mineral 36: 519–533